Thermal Testing of a Mars 2020 Enhanced Engineering Camera

Kaustabh Singh[1], Jason G. Kempenaar[2], and Keith S. Novak[3]
Jet Propulsion Laboratory, California Institute of Technology, Pasadena, CA 91109

The upcoming Mars 2020 rover mission is introducing a new generation of engineering cameras (ECAMs) called the enhanced engineering cameras (EECAMs), which have advanced imaging capability over the previous ECAMs used on the Spirit, Opportunity, and Curiosity rovers. The Mars 2020 rover will have nine EECAMs – six upgraded HazCams used for hazard avoidance, two upgraded NavCams used for navigation, and a single CacheCam used to take images of samples obtained by the rover's Sampling and Caching Subsystem (SCS). The detailed EECAM design was completed in April 2017, and since then the EECAM Subsystem has been in the process of fabrication, integration, and testing. This paper describes two thermal tests that were done for thermal model correlation and validation of the EECAM thermal design during Mars surface operations.

Nomenclature

AFT	=	Allowable Flight Temperature
CacheCam	=	Sample Caching Camera
COTS	=	Commercial Off-the-Shelf
DAQ	=	Data Acquisition System
ECAM	=	Engineering Camera
EDU	=	Engineering Development Unit
EECAM	=	Enhanced Engineering Camera
FM	=	Flight Model
GSE	=	Ground Support Equipment
HazCam	=	Hazard Avoidance Camera
JPL	=	Jet Propulsion Laboratory
MER	=	Mars Exploration Rover
MSL	=	Mars Science Laboratory
MTM	=	Mass-Thermal Model
NASA	=	National Aeronautics and Space Administration
NavCam	=	Navigation Camera
Ra	=	Rayleigh Number
RTD	=	Resistance Temperature Detector
SCS	=	Sampling and Caching Subsystem
STT	=	System Thermal Test
TC	=	Thermocouple
WCC	=	Worst-Case Cold
WCH	=	Worst-Case Hot

I. Introduction

THE upcoming Mars 2020 mission, scheduled to launch in July 2020, is currently undergoing integration and testing. Designed and built at the Jet Propulsion Laboratory (JPL) of the California Institute of Technology, one

[1] Thermal Engineer, Spacecraft Thermal Engineering, 4800 Oak Grove Dr., Pasadena, CA 91109, M/S 125-123
[2] Thermal Systems Engineer, Instrument and Payload Thermal Engineering, 4800 Oak Grove Dr., Pasadena, CA 91109, M/S 125-123
[3] Principal Engineer, Spacecraft Thermal Engineering, 4800 Oak Grove Dr., Pasadena, CA 91109, M/S 125-123

Copyright © 2019 California Institute of Technology

of the mission's primary goals is to search for conditions on Mars that could once sustain life. To improve the mission's risk and reduce costs, Mars 2020 is a build-to-print mission and heavily based on the design architecture of the Mars Science Laboratory (MSL) mission. The overall thermal design of the rover has largely remained the same, and has been covered in extensive detail in past papers.[1,2] Although most of the mission's hardware is build-to-print, the mission is utilizing new engineering cameras (ECAMs) called the enhanced engineering cameras (EECAMs). These EECAMs have improved imaging performance over the previous generation of ECAMs that were using on the MSL and Mars Exploration Rover (MER) missions. An overview of the EECAMs and their thermal design has been previously published.[3] Since this camera design is new, the EECAM team developed a flight-like engineering development unit (EDU) to reduce risk during integration and testing, and to verify electrical, mechanical, and thermal designs before protoflight testing and the rover System Thermal Test (STT).

One of the main limitations of validating the EECAM thermal design during protoflight testing or STT is the extent to which thermocouples could be instrumented on a flight camera unit. The cameras have warmup heaters used to warm the electronics and lens assemblies to their minimum operational temperature limits. As such, to properly assess the thermal performance of the cameras and characterize the key interfaces of these components, it was crucial to be able to instrument thermocouples on the internal electronics of the camera (particularly near the detector), as well as the lens assembly (particularly on the outermost glass lens element that takes the longest to warm up). The risk associated with putting thermocouples on these locations on a flight unit was deemed too high. The camera body interior is extremely space-constrained, and the only way to install any thermocouples would be to bond them down. Attempting to remove these bonded thermocouples post-test would be too intrusive, and there would not have been enough room to clip the wires and stake them down for flight. As for the outermost glass lens element, the main concern was that the installation and removal of a thermocouple would cause irreparable harm to the element and degrade the optical performance of the camera. As a result, to have a more complete validation of the thermal design, testing was done on the EDU rather than on an FM. There was an additional benefit that completing this test before any testing on flight units would provide time to make any necessary changes to the flight design. Waiting until STT or even protoflight testing would have meant less time to recover if any serious issues were found. Several months after the completion of the EDU test, a follow-up test was done on the EECAM thermal isolators used to interface with their mounting brackets.

II. EECAM EDU Thermal Test

A. Test Objectives

The thermal test of the EDU had five test objectives: 1) Demonstrate the electronic functionality of the EECAM EDU over the operational qualification temperature range (-70°C to 70°C), 2) Gather transient and steady-state warmup data for the (nearly) flight-like EECAM EDU, 3) Correlate the conductances and thermal capacitances of the EECAM thermal model to the transient and steady-state warmup data obtained from the test, 4) Use the correlated thermal model to update temperature predictions in the EECAM system thermal model, and 5) Characterize the warmup and maintenance heating of the EECAM using the EECAM EDU. All five test objectives were met. Test objective #1 was met during a thermal cycling test, which occurred in a 6 +/- 1 Torr GN_2 atmosphere. The remaining test objectives, #2-5, were met during a warmup characterization test. This warmup characterization test included transient and steady state testing (0.2°C/hr steady state criterion) in vacuum and 6 +/- 1 Torr GN_2 with heater operation to correlate the thermal model, to verify the effects of gas conductances, and to characterize the warmup and maintenance heating of the camera.

B. Thermal Test Configuration

1. Test Hardware

The EECAM EDU used for this thermal test was flight-like, with a few exceptions as listed in Table 1. In summary, most of the differences were minor and not enough to significantly change the overall thermal performance of the camera. Except for the detector frame that was made of a different aluminum alloy, the materials used in the EDU were identical to those of the flight models (FMs). The EDU dimensions, surface finishes, and torque values were also consistent with those of the FMs. No surface coatings were applied to the camera housing parts after they were machined. Most of the external surfaces of the FM camera housings are painted white, and thus have a high thermal emissivity. As a workaround to painting the parts to save time in schedule and processing, the EDU camera housing exterior was instead covered in Kapton tape ($\varepsilon = 0.8$), to achieve a higher emissivity over bare aluminum. Although some of the FM internal surfaces are black anodized (such as the detector frame and camera

housing internal faces), all the internal surfaces of the EDU were left as bare aluminum. Finally, the EDU camera housing had three total COTS heaters instead of a flight warmup heater. These three heaters were located on the same three sides of the mid-section/chassis as the flight heater would be located. Finally, depending on the test case, the EDU was mounted to the GSE bracket via either three M4 fasteners or three G10 thermal isolators. During flight, the FMs will be mounted to their brackets via three titanium isolators.

Mass-thermal models (MTMs) of the HazCam, NavCam, and CacheCam lenses were also developed as a means of testing the integration process. This thermal test utilized only the HazCam lens MTM since the HazCam is the most massive of all the EECAMs and is expected to have the longest warmup time. These lenses had the same dimensions, materials, interfaces, and thermal conductive paths as the flight lenses. Unlike the FMs, the glass lenses of these MTMs were not precision centered nor optically tested, but this was acceptable for a unit used in a thermal test. Although the FM lenses' internal surfaces are black anodized and external surfaces are painted white, the internal surfaces of the HazCam MTM were left as bare aluminum and the external surfaces were painted black with Z306. As with the camera housing, this was acceptable since the typical thermal emissivities of black paint (ε = 0.88) and white paint (ε = 0.9) are comparable. Table 1 lists out the major differences between the FMs and the EDU.

Table 1: Differences Between FMs and EDU

Design Feature	Flight Models	EDU
Detector Flexure Frame Material and Coating	Al 7075-T7351 (k = 155 W/m-K) Black Anodize (ε = 0.88)	Al 6061-T6 (k = 166 W/m-K) Bare Aluminum (ε = 0.1)
Camera Housing Surface Coatings	Interior: Black Anodized (ε = 0.88) Exterior: White Paint for Nav/HazCam (ε = 0.9) Bare Aluminum for CacheCam (ε = 0.1)	Interior: Bare Aluminum (ε = 0.1) Exterior: Kapton Tape (ε = 0.8)
Camera Heater	3x COTS Heaters (0.5" x 2", 156.8 Ω each)	1x Custom Heater (~18 mm x 188 mm, 34.4 Ω)
Heater Control	PRTs and Rover Flight Computer	Single Thermocouple and External On/Off Temperature Controller
Mounting Interface to Bracket	3x Titanium Flight Isolators	Either 3x M4 Fasteners or 3x G10 EDU Isolators
Lens Barrel Surface Coatings	Interior: Black Anodized (ε = 0.88) Exterior: White Paint for Nav/HazCam (ε = 0.9) Black Anodized for CacheCam (ε = 0.88)	Interior: Bare Aluminum (ε = 0.1) Exterior: Z306 Black Paint (ε = 0.88)

2. Test Setup

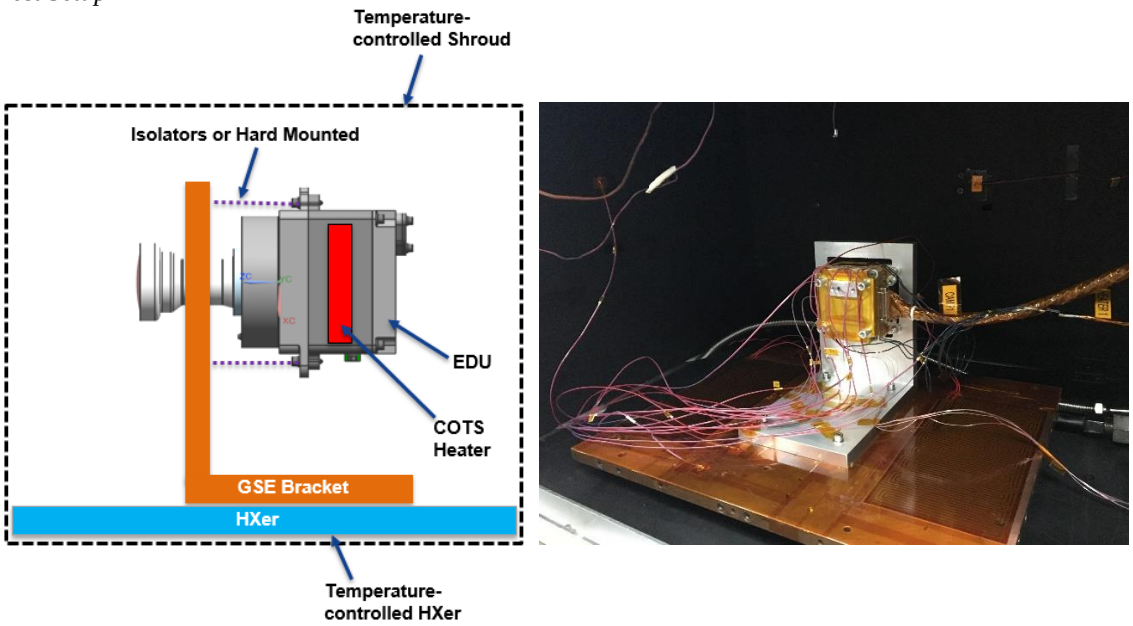

Figure 1: Test Article Setup in Chamber

The chamber had two thermal control zones: a temperature-controlled shroud and a temperature-controlled heat exchanger plate. During cooldowns when LN_2 flowed through the shroud and heat exchanger, a single thermocouple on the HXer was used to control both the shroud and heat exchanger since their fluid systems were connected to one another. During chamber warmups, however, the shroud and heat exchanger were controlled by their own individual TCs since they each had their own heaters.

The camera interfaced with the ground support equipment (GSE) bracket in either of two ways (see Figure 1). For the thermal cycling test cases, the camera was hard-mounted to the GSE using three M4 fasteners. For the warmup characterization test, the camera was mounted to the GSE bracket using three thermal isolators. The purpose of the isolators was to emulate the thermal interface between EECAMs and their brackets during flight. One of the test objectives was to characterize the warmup and maintenance heating of the EECAM using the development unit – in order to do so, the thermal interface needed to be as close to the flight configuration as possible. Since the flight-like isolators are difficult to machine and require special tooling for installation, they were not used during this thermal test. The isolator design can be seen in Figure 2.

The isolators used in flight are titanium flexures, while the thermal test isolator was stock G10 tubing that was cut to length. For each camera, three isolators are used at the interface with the bracket. The conductance of the flight isolators was calculated using $G = kA/L$, where k is the thermal conductivity of the material, A is the cross-sectional area of the isolator through which heat will flow, and L is the length of the isolator through which heat will flow. The calculated values were G = 0.0198 W/K for one titanium flight isolator and G = 0.0193 W/K for one G10 EDU isolator.

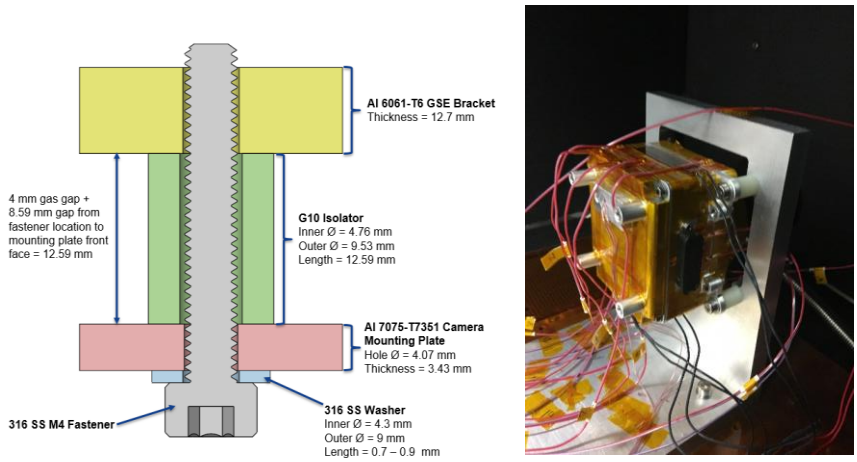

Figure 2: Cross-sectional View of EDU Thermal Isolator Design (Left); Image of EDU with Thermal Isolators Installed (Right)

3. Heaters

As aforementioned, the camera unit had three identical Kapton film heaters in approximately the same location where the flight heater will be – on three sides of the mid-section/chassis of the camera housing (see Figure 4). These heaters were powered at two wattages, 12 W and 20 W, and were used only during the warmup characterization test. As part of the warmup characterization test, the heaters were turned on and run out to steady state at 12 W in both vacuum and 6 +/- 1 Torr GN_2 environments. Once these portions of the test finished, a warmup and maintenance heating characterization was done with the heater power at 20 W, which is the lowest expected heater power during flight (occurring at a bus voltage of 28 V).

The heaters were powered with a power supply and controlled using an on/off temperature controller to accommodate the maintenance heating portion of Test Objective #5. The temperature controller used was capable of on/off heater control, similar to how the rover flight software computer-controlled heaters are configured. During the test, the controller was configured to have one of two setpoints: 60°C with a +/- differential of 3°C or -47°C with a +/- differential of 3°C.

4. Thermocouples

A total of 27 TCs were used for this thermal test. Two kinds of TCs were used: 6 feet long, 36 gauge, Type E TCs and 6 feet long, 26 gauge, Type E TCs. The smaller gauge thermocouples were used on the electronics. One TC was on the detector board, one was on the FPGA part case (on the middle board), and two were on the rear board (one at the center and one near the fastener). These internal TCs egressed through the HEPA filter hole, which had a diameter of 3.6 mm. One thermocouple, TC 12, was located on the center of the outermost glass element (Element 1) of the lens tube. Since Element 1 is the most massive element in the optics stack and is located furthest away from the camera body (where the heater is), it is the last element to warm up to the lens operating temperature. The

remaining 22 TCs were on the GSE, chamber, and exterior surfaces of the camera. Two TCs were located on the same area on the camera as the PRTs – one was used to log the hypothetical PRT temperature and the other was to control the camera heater. Table 2 shows a list of all the thermocouples used during the test program, not including the shroud and heat exchanger control thermocouples. The TCs that are highlighted had dedicated alarm limits, and the TCs in red are those that were on the electronics. The numbered thermocouple locations can be seen as green dots in Figure 3, Figure 4, and Figure 5.

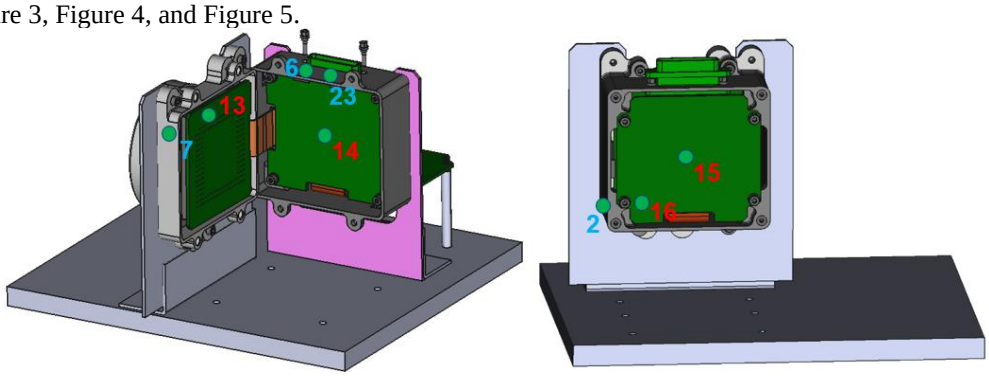

Figure 3: Internal Thermocouples on Camera

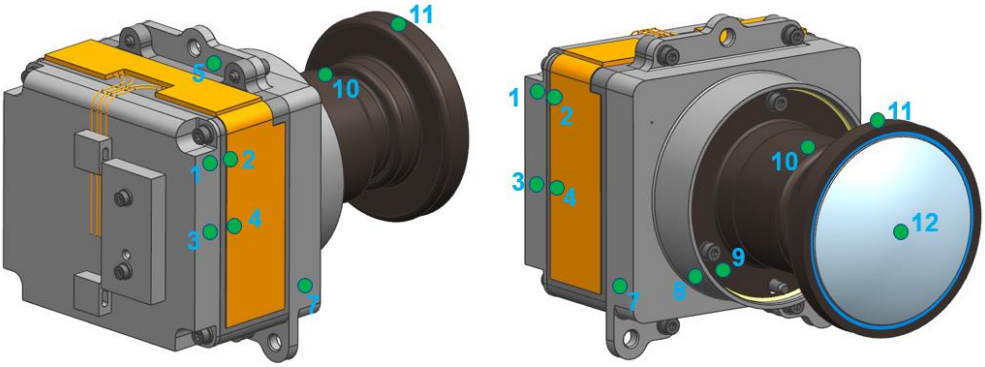

Figure 4: External Thermocouples on Camera

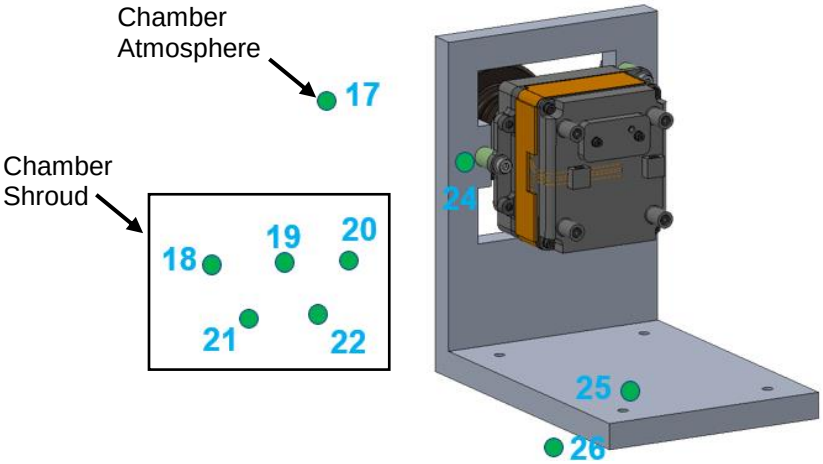

Figure 5: External Thermocouples on GSE and Chamber

Table 2: Thermocouple List

TC #	TC Name	Description	Min Non Op AFT (°C)	Max Op Qual (°C)	Alarm Limits (°C)	
					Low	High
1	TC1_RC_MS_Bolt_A	Bolt between RC & MS (RC Side)	-128	70	N/A	N/A
2	TC2_RC_MS_Bolt_B	Bolt between RC & MS (MS Side)	-128	70	-123	95
3	TC3_RC_MS_Contact_A	Contact between RC & MS (RC Side)	-128	70	N/A	N/A
4	TC4_RC_MS_Contact_B	Contact between RC & MS (MS Side)	-128	70	-123	95
5	TC5_MP_GSE_A	I/F between MP & GSE (MP Side)	-128	70	N/A	N/A
6	TC6_PRT	PRT Location (DAQ)	-128	70	N/A	N/A
7	TC7_Det_MP_Flexure_B	I/F between Detector & MP (MP Side)	-128	70	N/A	N/A
8	TC8_MP_Lens_Bolt_A	Bolt between MP & Lens (MP Side)	-128	70	N/A	N/A
9	TC9_MP_Lens_Bolt_B	Bolt between MP & Lens (Lens Side)	-128	60	N/A	N/A
10	TC10_Lens_Barrel_Half	Halfway Along Lens Barrel	-128	60	N/A	N/A
11	TC11_Lens_Barrel_End	End of Lens Barrel near Element 1	-128	60	N/A	N/A
12	TC12_E1_Center	Center of Element 1	-128	60	N/A	N/A
13	TC13_Det_MP_Flexure_A	I/F between Detector & MP (Det. Side)	-128	N/A	-123	100
14	TC14_Mid_Brd_FPGA	Center of Middle Board on FPGA	-128	N/A	-123	95
15	TC15_Rear_Brd_Center	Center of Rear Board	-128	N/A	-123	100
16	TC16_Rear_Brd_Bolt	Rear Board near Bolt	-128	N/A	N/A	N/A
17	TC17_Atm	Atmosphere/Ambient	N/A	N/A	N/A	N/A
18	TC18_Shroud_1	Shroud Surface 1	N/A	N/A	N/A	N/A
19	TC19_Shroud_2	Shroud Surface 2	N/A	N/A	N/A	N/A
20	TC20_Shroud_3	Shroud Surface 3	N/A	N/A	N/A	N/A
21	TC21_Shroud_4	Shroud Surface 4	N/A	N/A	N/A	N/A
22	TC22_Shroud_6	Shroud Surface 6	N/A	N/A	N/A	N/A
23	N/A	PRT Location (Temperature Controller)	-128	70	N/A	N/A
24	TC24_MP_GSE_B	I/F between MP & GSE (GSE Side)	N/A	N/A	N/A	N/A
25	TC25_GSE_HX_A	I/F between GSE & HXer (GSE Side)	N/A	N/A	N/A	N/A
26	TC26_GSE_HX_B	I/F between GSE & HXer (HXer Side)	N/A	N/A	N/A	N/A
27	TC27_EECAM_Cable	EECAM Cable near tie-down point	N/A	N/A	N/A	N/A

C. Test Matrix

The test was performed over a period of seven days. The test program was broken into two segments: thermal cycling testing and warmup characterization testing. The thermal cycling testing and warmup characterization testing were each three days long. Days 1 and 2 consisted of hot operational testing of the camera electronics at 70°C in a 6 +/- 1 Torr GN_2 environment. Day 3 consisted of cold operational testing of the camera electronics at -70°C in a 6 +/- 1 Torr GN_2 environment. After the first three days of testing, there was a chamber break on Day 4 to install the G10 thermal isolators onto the camera for the warmup characterization test. Day 5 consisted of a vacuum cool down to -100°C and warmup to steady state at 12 W and Day 6 consisted of a low pressure GN_2 cool down and warmup to steady state at 12 W. Day 7, the final day of testing, consisted of a flight-like warmup of the camera at 20 W to its minimum operational AFT.

Table 3: EDU Test Matrix

Test Case	Description	Atmosphere	Pressure (Torr)	HXer Setpoint (°C)	Camera Htr Setpoints (°C)	Camera Htr Power (W)	Camera Operation	Start Date and Time	End Date and Time	Duration
1.1a	Hot Functional Test #1	GN_2	6 +/-1	82	N/A	0	On	11/07/17 2:00 PM	11/07/17 6:40 PM	4 hrs 40 min
1.1b	Hot Functional Test #2	GN_2	6 +/-1	82	N/A	0	On	11/08/17 12:20 PM	11/08/17 4:50 PM	4 hrs 30 min
1.2	Cold Functional Test	GN_2	6 +/-1	-70	N/A	0	On	11/09/17 8:50 AM	11/09/17 2:30 PM	5 hrs 40 min
CHAMBER BREAK										
2.1	Vacuum Cool Down	Vacuum	~6E-5	-100	N/A	0	Off	11/13/17 6:30 PM	11/14/17 8:20 AM	13 hrs 50 min
2.2	Vacuum Warmup	Vacuum	~6E-5	-100	57 and 63	12	Off	11/14/17 8:20 AM	11/14/17 3:00 PM	6 hrs 40 min
2.3	GN_2 Cool Down	GN_2	6 +/-1	-100	N/A	0	Off	11/15/17 9:15 AM	11/15/17 1:10 PM	3 hrs 55 min
2.4	GN_2 Warmup	GN_2	6 +/-1	-100	57 and 63	12	Off	11/15/17 1:10 PM	11/15/17 5:55 PM	4 hrs 45 min
2.5	Vacuum Cool Down	Vacuum	~6E-5	-110	N/A	0	Off	11/15/17 6:10 PM	11/16/17 10:16 AM	16 hrs 6 min
2.6	GN_2 Flight-like Warmup	GN_2	6 +/-1	-110	-50 and -44	20	Off/On	11/16/17 10:16 AM	11/16/17 1:40 PM	3 hrs 24 min

D. Test Results

During the thermal cycling portions of the test, two types of camera operational tests were done: a short functional test and a regression test. The short functional test was essentially a checkout of the various camera electronic components to verify functionality. Short functional tests were performed whenever a configuration of the

chamber was changed, such as whenever the door was closed, a pump down occurred, or a backfill occurred. The regression tests involved taking images using the camera in various modes, similar to how it will operate during flight. These tests were done during the thermal cycling test, at the camera's operating qualification temperatures of 70°C and -70°C. The short functional and regression testing was successfully completed at both of these hot and cold operational temperature limits.

Once the thermal functional testing was completed, the chamber was opened to install the G10 thermal isolators onto the camera. Afterwards, the chamber was pumped down to vacuum, cooled down, and the camera heaters were turned on. At steady state, there was approximately a 22°C gradient across the entirety of the camera, with the maximum temperature right where the heaters were located and the minimum temperature at the center of the glass lens element. This maximum gradient was about 13°C lower than original model predictions showed. The maximum camera temperature was about 25°C warmer than originally predicted. Similarly, the GN_2 steady state gradients were lower than model predictions while the maximum camera temperature was about 15°C warmer than expected. These smaller gradients showed that the actual thermal conductances at the various camera interfaces were higher than previously assumed for thermal analysis. The warmer steady state temperatures were due to the overall warmer environments than previously assumed. While the heat exchanger plate and two of the shroud surfaces did cool down to -100°C, the gradients in the shroud were higher than expected. Three shroud surfaces only cooled to -85°C. Additionally, the thermal isolation of the G10 isolators was higher than originally calculated, as explored further in the model correlation section. Camera and GSE temperatures for the vacuum and GN_2 characterization testing can be seen in Figure 6 and Figure 7, respectively.

For the final test, the camera was cooled down to -95°C in a GN_2 atmosphere. The camera heaters were turned on at 20 W with on/off setpoints of -50°C and -44°C. By 15 minutes later, all the camera TCs had reached their operational AFTs (-55°C for the camera body and -95°C for the lens assembly). Figure 8 shows the temperatures of the internal components and lens assembly, with the TC near the PRT location for context. Additionally, the camera was turned on during maintenance heating to see the effect of heat dissipation on the heater performance. With the camera off, the duty cycle was about 27%. When on, the duty cycle decreased to 25%. To increase the electronics' temperatures as much as possible, the camera was made to take images in its most power-consuming settings, even though the camera would never be operated that way during flight. After all the temperatures settled, the duty cycle had decreased to 22%. As such, the duty cycle would decrease by approximately 5% when the camera is operated under its most thermally-stressful conditions, showing that the dissipation of the camera does not significantly interfere with the heater performance with a control PRT located on the housing.

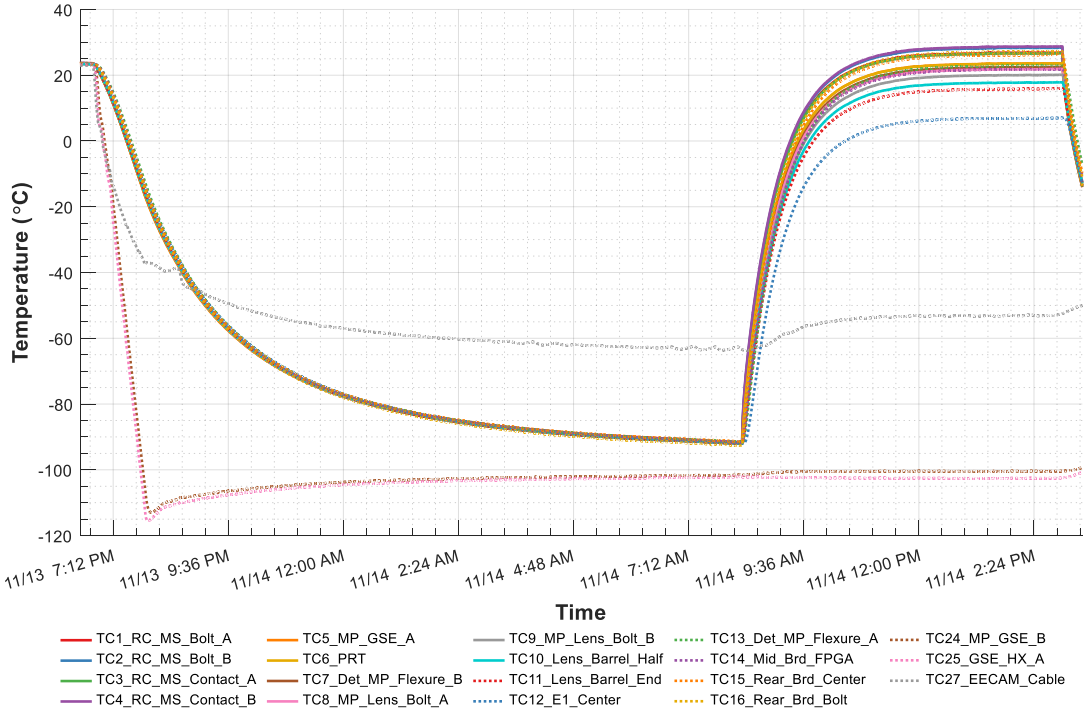

Figure 6: Cases 2.1 & 2.2, Vacuum Cool Down and Steady State Warmup – Camera and GSE TCs

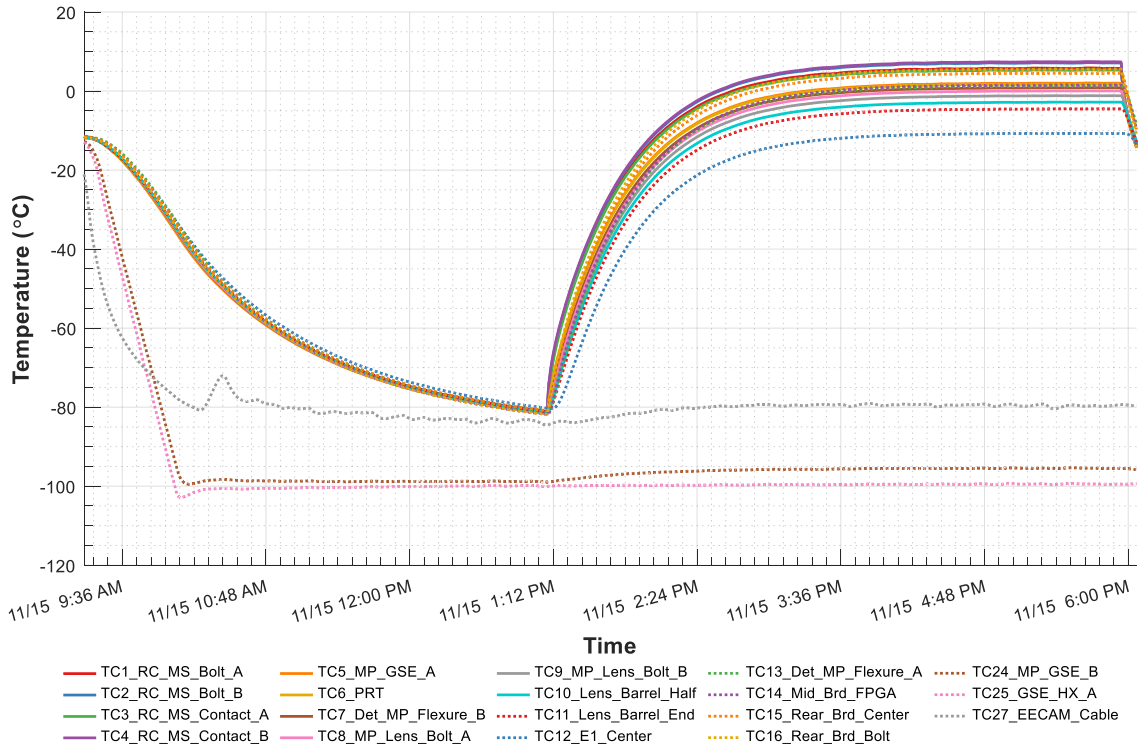

Figure 7: Cases 2.3 & 2.4, 6 Torr GN_2 Cool Down and Steady State Warmup – Camera and GSE TCs

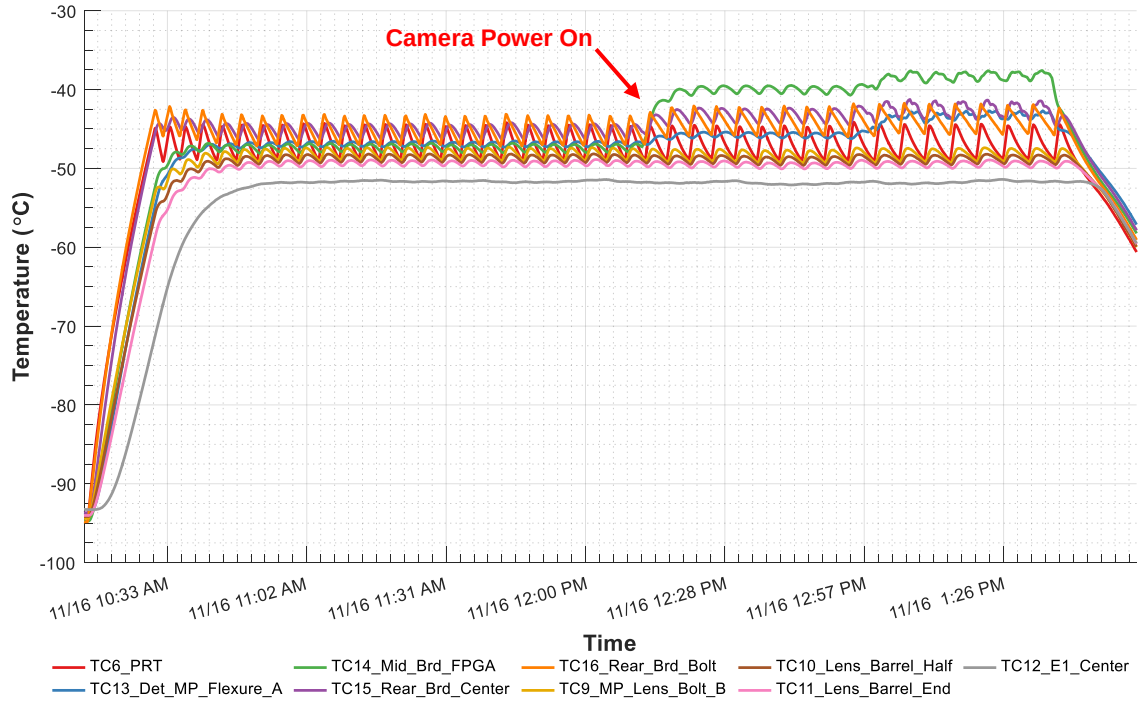

Figure 8. Case 2.6, 6 Torr GN_2 Flight-like Warmup – Internal and Lens TCs

E. Thermal Model Correlation

A thermal model of the camera was correlated to the test data from TCs 1-16, TC 24, and TC 25. These include all camera and GSE TCs, with the exception of TC 27 on the EECAM power cable. The remaining thermocouples, TCs 17-22, TC 26, and TC 27 were used as input environmental boundary conditions to assist in the correlation. These include the atmosphere TC, all the TCs on shroud surfaces, the EECAM cable TC (since it was located on the cable's tie-down point to the shroud), and the heat exchanger plate TC. A total of 18 TCs had to be correlated to data, and prioritization was done to correlate more crucial TCs, such as the electronics TCs, lens TCs, and the PRT TC. Only the warmup characterization test data was used for model correlation. The correlation was done in the following order: vacuum steady state, vacuum transient, 6 Torr GN_2 steady state, 6 Torr GN_2 transient, and 6 Torr GN_2 flight-like warmup. For the vacuum and GN_2 steady state and transient data, the goal was to correlate steady state and transient temperatures to within 5°C of the test data. For the GN_2 flight-like warmup, the goal was to correlate the warmup temperatures to within 5°C of the test data and to correlate the heater duty cycle to within 5% that of the test data. Another goal for all the correlation was to try and make sure the correlated results were slightly more conservative than what the test data shows, to maintain some margin. A full list of all model changes is shown in Table 4.

Table 4: Thermal Model Values Before and After Correlation

	Initial Value		**Final Value**	
Parameter	**Vacuum**	**6 Torr GN_2**	**Vacuum**	**6 Torr GN_2**
Thermal Isolator Conductance (Per Isolator)	0.0193 W/K	0.0193 W/K	0.0043 W/K	0.0089 W/K
Bolted-joint and RTV Conductance Between Mounting Plate and Lens Assembly (Per M2.5 Fastener)	0.097 W/K	0.097 W/K	0.32 W/K	0.32 W/K
Detector Board to Middle Board Flex Cable Conductance	0.03 W/K	0.03 W/K	0.0064 W/K	0.0064 W/K
Middle Board to Rear Board Flex Cable Conductance	0.037 W/K	0.037 W/K	0.0077 W/K	0.0077 W/K
Detector Board Thickness	1.59 mm	1.59 mm	2.03 mm	2.03 mm
Middle Board Thickness	1.59 mm	1.59 mm	1.88 mm	1.88 mm
Rear Board Thickness	1.59 mm	1.59 mm	1.88 mm	1.88 mm
Bolted-joint Conductance Between GSE Bracket and HXer Plate (Per M5 Fastener)	0.3 W/K	0.3 W/K	1.5 W/K	1.5 W/K
Bolted-joint Conductance Between Rear/Middle Boards and Camera Housing (Per M2.5 Fastener)	0.2 W/K	0.2 W/K	0.15 W/K	0.15 W/K
Detector to Mounting Plate I/F Conductance	0.14 W/K	0.14 W/K	0.14 W/K	0.14 W/K
Rear Cover Density Multiplier	1.2	1.2	1.8	1.8
Mid-Section/Chassis Density Multiplier	2.4	2.4	1.7	1.7
Mounting Plate Density Multiplier	3.1	3.1	1.4	1.4
Rear Board Density Multiplier	3.2	3.2	1.4	1.4
Middle Board Density Multiplier	3.5	3.5	2.2	2.2
Detector Board Density Multiplier	1.7	1.7	1.4	1.4
Camera Convection Coefficient	0 W/m^2-K	0.75 W/m^2-K	0 W/m^2-K	0.8 W/m^2-K
Camera Cable Convection Coefficient	0 W/m^2-K	3 W/m^2-K	0 W/m^2-K	3 W/m^2-K
GSE Bracket Convection Coefficient	0 W/m^2-K	1.5 W/m^2-K	0 W/m^2-K	1.5 W/m^2-K

For the most part, the model correlation went very well. Nearly all vacuum steady state temperatures were correlated to within 2°C of the test data. The exception to this was the TC 6 (PRT) temperature. At vacuum steady state, the model reads a temperature about 3.2°C colder than what the test data shows. However, this was acceptable because it was within the goal of a < 5°C model error. Furthermore, the PRT temperature reading colder was more conservative for the warmup of the camera. Since this correlated model will eventually be used to develop heater tables for flight operations, maintaining some margin in the PRT temperature was beneficial. The final results of the vacuum steady state correlation can be seen in Table 5.

Table 5: Vacuum and GN Steady State Correlation Results

	Vacuum Correlation			GN_2 Correlation		
TC Name	**Steady State Test Temperature (°C)**	**Steady State Model Temperature (°C)**	**$T_{model} - T_{test}$ (°C)**	**Steady State Test Temperature (°C)**	**Steady State Model Temperature (°C)**	**$T_{model} - T_{test}$ (°C)**
TC1_RC_MS_Bolt_A	26.9	26.3	-0.6	5.7	6.1	0.3
TC2_RC_MS_Bolt_B	28.4	27.1	-1.3	7.1	6.7	-0.4
TC3_RC_MS_Contact_A	26.7	25.7	-1.0	5.3	5.5	0.2
TC4_RC_MS_Contact_B	28.8	27.2	-1.5	7.4	6.9	-0.5
TC5_MP_GSE_A	23.6	23.8	0.2	2.0	2.6	0.6
TC6_PRT	23.6	20.4	-3.2	1.7	-0.3	-2.0
TC7_Det_MP_Flexure_B	22.6	21.5	-1.1	0.8	0.3	-0.5
TC8_MP_Lens_Bolt_A	21.9	21.1	-0.8	0.0	0.4	0.4
TC9_MP_Lens_Bolt_B	20.2	18.9	-1.2	-1.2	-1.5	-0.3
TC10_Lens_Barrel_Half	17.8	16.4	-1.5	-2.8	-3.7	-0.9
TC11_Lens_Barrel_End	15.9	14.7	-1.2	-4.5	-5.1	-0.6
TC12_E1_Center	7.0	7.9	0.9	-10.7	-10.2	0.5
TC13_Det_MP_Flexure_A	23.0	22.7	-0.3	1.3	1.8	0.5
TC14_Mid_Brd_FPGA	21.9	23.8	1.9	1.5	3.2	1.7
TC15_Rear_Brd_Center	26.3	25.0	-1.2	4.5	4.5	0.0
TC16_Rear_Brd_Bolt	27.2	26.6	-0.6	5.5	6.2	0.7
TC24_MP_GSE_B	-100.4	-100.1	0.3	-95.5	-94.2	1.3
TC25_GSE_HX_A	-102.5	-102.1	0.4	-99.5	-98.6	0.8

Similarly, all the GN_2 steady state temperatures were correlated to within 2°C of the test data, with no exceptions. As with its vacuum counterpart, the GN_2 steady state temperature of TC6_PRT in the model was slightly colder than what the test data showed. As mentioned, this was done to maintain some conservatism in the model. More effort was put forth into correlating the GN_2 temperature results since during flight the cameras won't be operating in vacuum, they will be operated in a CO_2 atmosphere. For this reason, it was crucial to make sure all the gas conductances were modeled appropriately. The final results of the GN_2 steady state correlation can also be seen in Table 5.

All the cooldown and warmup transient temperatures were correlated very well against the test data for both the vacuum and GN_2 cases. All transient data was correlated to within 5°C of the test results. The final case to correlate was the GN_2 flight-like warmup. There were two objectives: to correlate the transient warmups to < 5°C, and to correlate the duty cycle of the thermal model's heater to within 5% of the camera heater duty cycle during the test. Although part of the maintenance heating included operation of the camera, only the duty cycle during the non-operational period was used as a correlation point. Accurate power dissipation values for the operation of the camera were not available at the time to correlate this portion, and this additional operational case was only done to see the sensitivity of the heater to the power dissipation of the electronics. There was not much of a concern in correlating the transient warmups to much better than < 5°C. A temperature difference of 5°C only registers as a warmup time difference of 1-2 minutes since the camera heaters put 20 W into the camera. No additional model changes were needed to further correlate the GN_2 flight-like warmup case beyond what was done during the GN_2 steady state correlation. Almost all warmup transients matched within 5°C and the thermal model heater's duty cycle was only 3% off from that of the test heaters (test heaters' duty cycle was 27%, thermal model heater's duty cycle was 30%). The exception to this was that the TC on the detector board had an error as high as 5.5°C during the warmup. However, this was done on purpose to maintain some conservatism since the detector/detector board are the last components to warm up to their AFT of -55°C. Furthermore, the detector interfaces with the mounting plate via a flexure frame. Although the flexure frames of the FMs are made of Al 7075, the frame used for this test was made of Al 6061. Since Al 6061 has a higher thermal conductivity than Al 7075, the actual interface conductance for a flight configuration would be slightly less. The fact that the flight-like warmup results matched so well was a promising validation of all the prior vacuum and GN_2 correlation. Table 6 shows a comparison between the model and test warmup times to -55°C for all the camera TCs. The lens assembly (TCs 9 to 12) does not have a minimum operational AFT -55°C, but its TCs are also included in the table for a point of reference since the warmup was started above its minimum operational AFT of -95°C.

Table 6: GN_2 Flight-like Warmup Results – Case 2.6

TC Name	Description	Warmup Time to -55°C (min)		Model Time – Test Time (min)
		Test	Model	
TC1_RC_MS_Bolt_A	Bolt between RC & MS (RC Side)	7.2	8.6	1.4
TC2_RC_MS_Bolt_B	Bolt between RC & MS (MS Side)	6.9	8.5	1.6
TC3_RC_MS_Contact_A	Contact between RC & MS (RC Side)	7.5	8.7	1.2
TC4_RC_MS_Contact_B	Contact between RC & MS (MS Side)	6.6	7.8	1.2
TC5_MP_GSE_A	I/F between MP & GSE (MP Side)	10	10.2	0.2
TC6_PRT	PRT Location (DAQ)	10.2	11.7	1.5
TC7_Det_MP_Flexure_B	I/F between Detector & MP (MP Side)	11.4	11.9	0.5
TC8_MP_Lens_Bolt_A	Bolt between MP & Lens (MP Side)	12.2	12.4	0.2
TC9_MP_Lens_Bolt_B	*Bolt between MP & Lens (Lens Side)*	*13.2*	*14.2*	*1*
TC10_Lens_Barrel_Half	*Halfway Along Lens Barrel*	*14.4*	*16.5*	*2.1*
TC11_Lens_Barrel_End	*End of Lens Barrel near Element 1*	*16.8*	*18.8*	*2*
TC12_E1_Center	*Center of Element 1*	*24.6*	*26.9*	*2.3*
TC13_Det_MP_Flexure_A	I/F between Detector & MP (Det. Side)	15.1	15.9	0.8
TC14_Mid_Brd_FPGA	Center of Middle Board on FPGA	14.2	13.9	-0.3
TC15_Rear_Brd_Center	Center of Rear Board	10.5	12	1.5
TC16_Rear_Brd_Bolt	Rear Board near Bolt	9.3	9.3	0

One interesting result from the correlation is that the conductance of the G10 thermal isolator was lower than previously calculated (see Table 4). The initial assumption was that the fastener at the center of the isolator would have good contact against the camera and bracket, and thus cause a thermal short from the camera to the bracket. The fastener and G10 conductances were calculated using a 316 Stainless Steel thermal conductivity of 16.2 W/m-K and a G10 thermal conductivity of 0.74 W/m-K. These conductances in parallel lead to a total conductance of 0.015 W/K, per isolator. At the time, the conductance of each flight isolator was estimated to be 0.013 W/K. The correlated value, however, was about 3x less at 0.0043 W/K in the vacuum case, and was about 2x less at 0.0089 W/K in the GN_2 case. This suggests that the fastener, in fact, did not have good contact with both the camera and bracket. More so, taking the extreme case in vacuum and assuming the no heat conduction through the fastener, one could back-calculate what the thermal conductivity of the G10 would be if all the heat flowed only through the G10. This conductivity ends up being about 1 W/m-K, which is slightly higher than typical values one could expect to find for G10 (0.5 to 0.8 W/m-K). This suggests that in the vacuum case while most of the heat flowed through the G10, some of it did indeed flow through the fastener. The heat flow through the fastener just ended up being less than previously assumed. With the addition of GN_2, the contact resistance between the fastener and camera/bracket decreases, increasing the overall conductance. As a follow-up to the EDU Thermal Test, an additional thermal test was done to verify the correlated values of the G10 isolators and to test the conductance of the flight titanium isolators.

III. EECAM Thermal Isolator Test

A. Test Objectives

The thermal isolator test had three objectives: 1) Gather vacuum, CO_2, and GN_2 steady-state warm up data for the EECAM EDU isolator (G10) and EECAM flight isolator (Ti), and calculate their conductances, 2) Use calculated EECAM EDU isolator (G10) conductances to compare against correlations of the EECAM EDU Thermal Test, 3) Use calculated EECAM flight isolator (Ti) conductances to update flight temperature predictions in the EECAM system thermal model. All three test objectives were met. Test objective #1 was met during the steady-state testing which occurred at several temperatures and in several environments. Test objective #2 was met when the G10 isolator results of the test were used to compare against the correlated EECAM EDU test results, and test objective #3 was met when the Ti isolator results were used to update flight predictions of the EECAMs.

B. Thermal Test Configuration

1. Test Hardware

A total of four isolators were used in this thermal test: two G10 EDU isolators and two titanium (Ti-6Al-4V) isolators. Pairs of each isolator type were tested because, as isolators, a relatively small amount of heat flow across the isolators results in a large temperature gradient. Original test configurations with only one of each isolator had issues where the total required power would have been too small compared to the parasitic heat loads and accuracy

of the power supply. Two of the three G10 isolators from the EDU test were re-used for this test. A few views of the titanium isolator design can be seen in Figure 9. Based on the geometry and configuration, the expected conductance of the titanium isolator was anywhere from 0.0109 W/K to 0.0135 W/K, depending on the assumed titanium conductivity and environment (vacuum, CO2, or GN2). The two titanium isolators that were tested were nearly identical to the flight design. The flexure surfaces (highlighted blue in Figure 9) were electrical discharge machined, the result of which is a recast layer that needs to be removed from the flight isolators. The isolators that were tested, however, did not have their recast layer removed. Since typical thicknesses of recast layers are on the order of a 1/10 of a thousandth of an inch, this recast layer was not enough to significantly affect the isolators' performance.

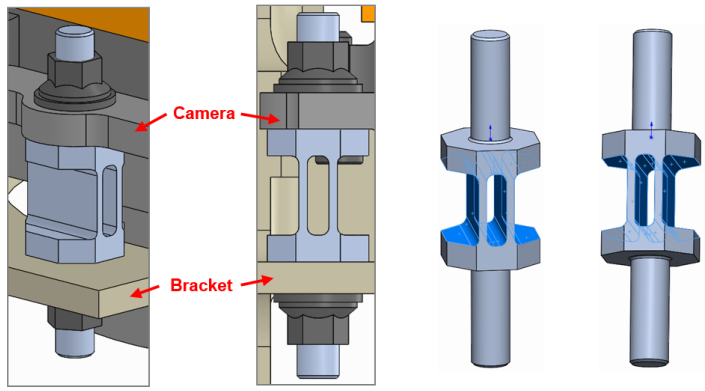

Figure 9: Views of Titanium Flight Isolators

2. Test Setup

A schematic of the test setup can be seen in Figure 10. At the center of the test setup were two heater plates. Each heater plate had one pair of the isolators to be tested – one plate had the two titanium isolators and the other had the two G10 isolators. Additionally, each heater plate had a 10-Ω Dale Ohm resistor and an RTD. The heater plates were controlled to about room temperature and mounted to the adapter plate, which had an RTD at the mounting interface of each isolator pair. Enveloping the entire test apparatus (the heater plates and adapter plate) was an SLI enclosure made of double-aluminized Mylar. The SLI enclosure had three main purposes. First, it was meant to limit radiative heat transfer between the heater plates and the room. Second, it was sized small enough around the test setup to ensure that during gas testing no convection cells would form, and only gas conduction would be present.[4] Third, the SLI enclosure was designed to track as closely to room temperature as possible – for this reason, the exterior faces of the enclosure were covered in black Kapton tape.

The chamber had one thermal control zone that was used, a cold plate heat exchanger that was connected to a chiller via insulated fluid lines. The cold plate sat inside the chamber on Teflon standoffs that were built to provide conductive isolation between the cold plate and chamber floor. The control point for this zone was inside the chiller itself, which was controlled between ~-30°C and ~-70°C during the steady state testing. The adapter plate with the heater plates, isolators, and SLI enclosure was bolted onto the cold plate via four M5 fasteners.

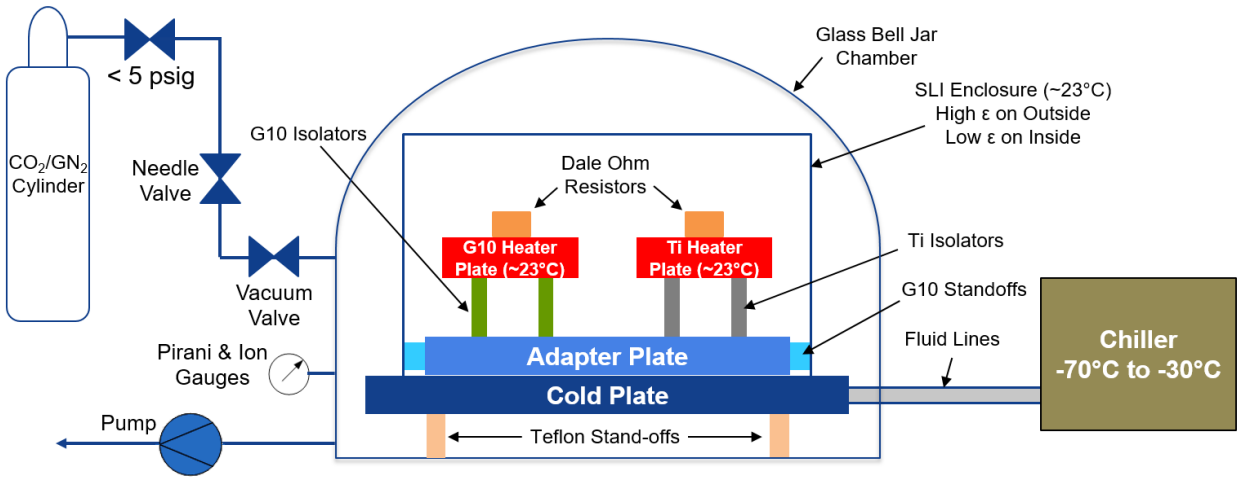

Figure 10: Schematic of Thermal Isolator Test Setup

3. Heaters

As mentioned earlier, each heater plate had a single 10-Ω Dale Ohm resistor bonded to it. Each heater was controlled individually in separate heater zones, by separate power supplies. Table 7 shows some of the heater characteristics during the steady state testing.

Table 7: Heater Characteristics

Heater Zone/Location	Number of Heaters	Heater Resistance	Heater Voltage	Heater Current	Heater Power
G10 Heater Plate	1	10 Ω	2.77 V (min)	0.27 A (min)	0.75 W (min)
			4.4 V (max)	0.429 A (max)	1.89 W (max)
Ti Heater Plate	1	10 Ω	3.58 V (min)	0.348 A (min)	1.24 W (min)
			5.2 V (max)	0.505 A (max)	2.63 W (max)

4. Temperature Sensors

A total of nine temperature sensors were used for this thermal test: five type K TCs and four RTDs. Four of the TCs were placed around the SLI enclosure while the last TC was used to measure the gas temperature inside the enclosure during atmospheric testing. Because of their higher accuracy, the four RTDs were placed on the heater plates and adapter plate. The RTDs were routed through the power feedthrough via the remaining eight of the 12 total leads. The TC and RTD locations can be seen in Figure 11.

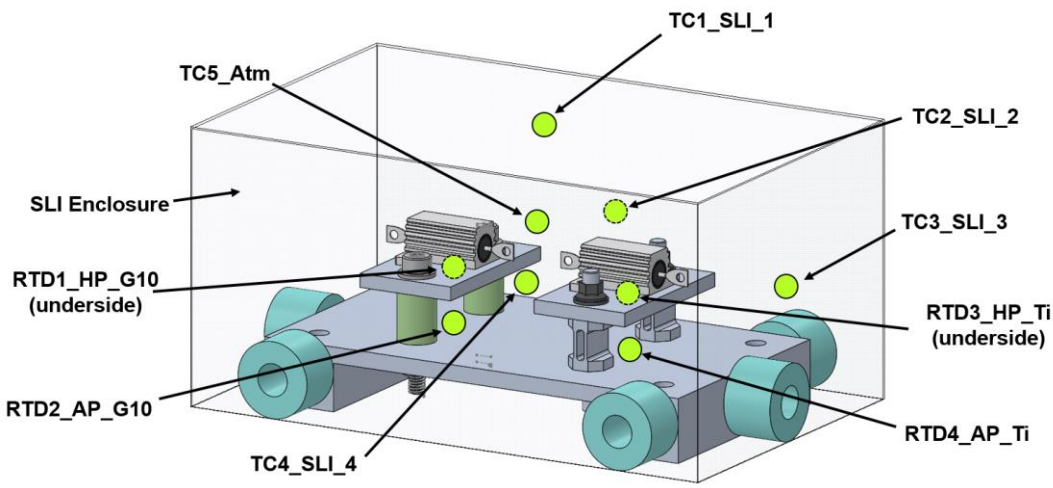

Figure 11: Thermocouple and RTD Locations

C. Test Matrix

The test was performed over a period of three days. The first day involved vacuum testing, the second day involved CO_2 testing, and the third day involved GN_2 testing. For each environment, three test cases were done in which the chiller was controlled to -30°C, -50°C, and -70°C. At each of these temperatures, each heater's power was adjusted until both heater plates were at about room temperature. The purpose of running the heater plates at room temperature was to maximize the temperature difference between the heater plates and adapter plate, making the parasitic heat transfer between the heater plates and environments as small a percentage of the total heat flow through the isolators as possible. Doing so also helped with improving the relative accuracy of the results. After the heater power was enough to stabilize the temperatures at room temperature, each test case was completed once the steady state criterion of 0.2°C/hr was met.

For testing in gaseous environments, the goal was to do testing in 6 Torr of CO_2 and 6 Torr of GN_2. Some issues arose during the test that prevented those conditions from being precisely met – however, the resulting environments were still acceptable to get usable results. For low pressure non-vacuum testing, a Pirani gauge was used to measure the chamber pressure. However, due to some pressure readings that did not make sense, it was discovered, after the CO_2 testing was completed, that the readings from Pirani gauges are dependent on the gas inside of the chamber. Pirani gauges have a hot filament, and the rate at which heat is lost from the filament to the gas chamber is used to

determine what the pressure is. Therefore, the pressure reading depends on the gas conductivity and the gauge/measurement system needs to be calibrated to that gas. Typically, by default, Pirani gauges and their controllers are calibrated to nitrogen. Consequently, although it was believed that testing was done in 6 Torr CO_2, the chamber was actually in the 10 to 20 Torr range because the Pirani gauge and its controller was calibrated to nitrogen while CO_2 was in the chamber. The testing at 10 to 20 Torr vs 6 Torr did not significantly affect any test results. Since the thermal conductivity of gases is independent of pressure (until the pressure is low enough that free molecular flow dominates), the higher pressure testing really only affected the gas gap at which convection would have started to occur. Whether or not convection occurred really only affected the parasitic heat load calculations to determine what portion of the heater plate heat balance was actually conduction through the thermal isolators. This was determined using the Rayleigh number, *Ra*. For small Rayleigh numbers (< ~10^3) heat transfer is primarily driven by conduction across the fluid and convection cells do not form. To validate the results, the Rayleigh number was evaluated for each surface pairing that involved a heater plate in each of the three CO_2 test cases. These surface pairings included each individual heater plate with the SLI surfaces, the heater plates to the adapter plate, and heater plate to heater plate. The Rayleigh number was evaluated at pressures from 6 Torr to 100 Torr to see its variation across that range and verify how much margin there was to the onset of convection. The highest Rayleigh numbers occurred in the -70°C CO_2 case. For this temperature range, a Rayleigh number of 1000 was only reached at a pressure of ~65 Torr, showing that there was plenty of margin from the conservative maximum 20 Torr pressure that was reached during the test. At 20 Torr, the calculated Rayleigh number was only 100. There is some uncertainty to the required 1000 Rayleigh number for convection to start – however, assuming that it could start at an even lower value such as 600, such a Rayleigh number wouldn't be achieved until about 50 Torr of CO_2. Therefore, there was analytical evidence that convection did not occur inside the SLI enclosure during any of the 10-20 Torr CO_2 testing. The full test matrix can be seen in Table 8.

Table 8: Thermal Isolator Test Matrix

Test Case	Description	Atmosphere	Pressure (Torr)	Average Adapter Plate Temperature (°C)	G10 Heater Plate Temperature (°C)	G10 Heater Plate Power (W)	Ti Heater Plate Temperature (°C)	Ti Heater Plate Power (W)	Duration
1.1	Vacuum, -30°C Chiller	Vacuum	6 +/-1	-31.1	20.6	0.75	21.1	1.24	2 hrs 37 min
1.2	Vacuum, -50°C Chiller	Vacuum	6 +/-1	-52	20.6	1.04	20.3	1.68	2 hrs 31 min
1.3	Vacuum, -70°C Chiller	Vacuum	6 +/-1	-69.6	21.7	1.29	21.9	2.1	2 hrs 28 min
2.1	CO_2, -70°C Chiller	CO_2	10-20	-65.8	20.5	1.43	22	2.27	4 hrs 50 min
2.2	CO_2, -50°C Chiller	CO_2	10-20	-49.5	21.1	1.19	22.1	1.88	2 hrs 34 min
2.3	CO_2, -30°C Chiller	CO_2	10-20	-29.6	21.5	0.88	22.5	1.4	2 hrs 38 min
3.1	GN_2, -30°C Chiller	GN_2	6 +/-1	-30.6	18.9	1.06	19.7	1.56	1 hr 56 min
3.2	GN_2, -50°C Chiller	GN_2	6 +/-1	-51.2	19.6	1.51	19.7	2.16	1 hr 47 min
3.3	GN_2, -70°C Chiller	GN_2	6 +/-1	-68.6	20.9	1.89	19.6	2.63	1 hr 48 min

D. Test Results

As aforementioned, the EECAM Isolator Thermal Test occurred over the course of three days. Temperature measurements for all test cases can be seen in Figure 12. In determining the conductances of the isolators, solely using the heater plate powers could not be done. A heat flow balance about each of the heater plates was done to determine what percent of the heater input actually conducted through the isolators compared to the parasitic heat load contributions due to the environment. There were two sources of parasitic heat flows: gas conduction and radiation. Gas conduction was evaluated using the gas conductivity as determined by the average temperature of the two surfaces being analyzed, as well as the distance between the respective surfaces. Radiative heat flow was calculated in two parts. First, a simple thermal model of the test setup was built to calculate the radiation conductances of the entire test setup. Then, these radiation conductances were used together with the surface temperatures to evaluate the net radiative heat flow. As expected, the percent parasitic heat loads were higher for the G10 isolators since their thermal resistance was higher than that of the Ti isolators. A peak percentage of 10% occurred for the G10 isolators in the -70°C GN_2 case. The peak parasitic heat load percentage for the Ti isolator was 6.2% and occurred in the same test case. With the parasitic heat loads accounted for, the remaining heater power was that which conducted through the isolators. Table 9 shows the total parasitic heat loads and Table 10 lists out all the final isolator conductances.

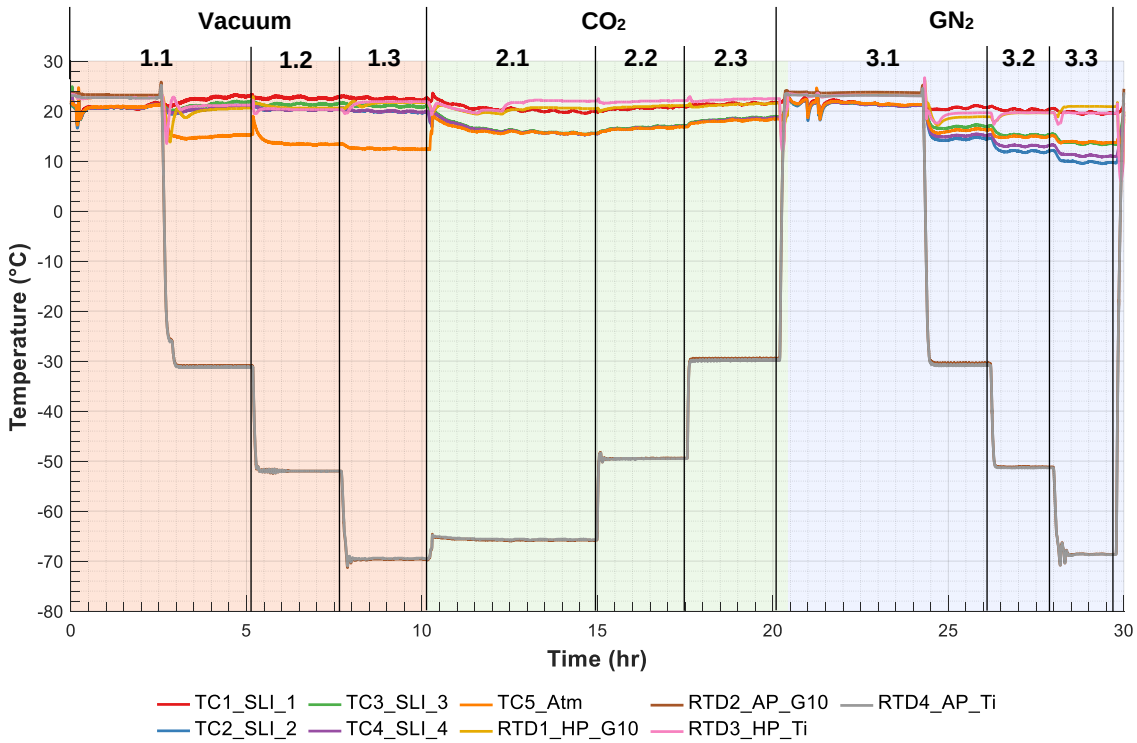

Figure 12: Thermal Isolator Test TC and RTD Measurements

Table 9: Parasitic Heat Loads

Value	Vacuum -30°C	Vacuum -50°C	Vacuum -70°C	CO_2 -30°C	CO_2 -50°C	CO_2 -70°C	GN_2 -30°C	GN_2 -50°C	GN_2 -70°C
G10 Heater Power (W)	0.74	1.01	1.27	0.86	1.17	1.41	1.05	1.48	1.86
G10 Total Parasitic Heat (W)	0.0087	0.0117	0.0149	0.068	0.0887	0.1035	0.1009	0.1455	0.1843
G10 Parasitic Heat as % of Heater Power (%)	1.2%	1.2%	1.2%	7.9%	7.6%	7.3%	9.6%	9.8%	9.9%
G10 Isolator Conduction (W)	0.73	1.00	1.25	0.79	1.09	1.30	0.95	1.34	1.67
Ti Heater Power (W)	1.22	1.65	2.06	1.38	1.85	2.22	1.54	2.12	2.58
Ti Total Parasitic Heat (W)	0.0094	0.0114	0.0151	0.066	0.0853	0.1001	0.0959	0.1316	0.1595
Ti Parasitic Heat as % of Heater Power (%)	0.8%	0.7%	0.7%	4.8%	4.6%	4.5%	6.2%	6.2%	6.2%
Ti Isolator Conduction (W)	1.21	1.64	2.05	1.31	1.76	2.12	1.44	1.99	2.42

Table 10: Final Isolator Conductances

Value	Vacuum -30°C	Vacuum -50°C	Vacuum -70°C	CO_2 -30°C	CO_2 -50°C	CO_2 -70°C	GN_2 -30°C	GN_2 -50°C	GN_2 -70°C
RTD1_HP_G10 (°C)	20.6	20.6	21.7	21.5	21.1	20.5	18.9	19.6	20.9
RTD2_AP_G10 (°C)	-31	-52	-69.6	-29.5	-49.4	-65.8	-30.4	-51.2	-68.6
G10 Isolator Conduction (W)	0.73	1.00	1.25	0.79	1.09	1.30	0.95	1.34	1.67
Conductance Per G10 Isolator (W/K)	**0.0068**	**0.0066**	**0.0064**	**0.0076**	**0.0075**	**0.0073**	**0.0094**	**0.0093**	**0.0092**
RTD3_HP_Ti (°C)	21.2	20.3	21.9	22.5	22.1	22	19.7	19.7	19.6
RTD4_AP_Ti (°C)	-31.2	-52	-69.5	-29.8	-49.5	-65.7	-30.8	-51.3	-68.7
Ti Isolator Conduction (W)	1.21	1.64	2.05	1.31	1.76	2.12	1.44	1.99	2.42
Conductance Per Ti Isolator (W/K)	**0.0116**	**0.0113**	**0.0112**	**0.0125**	**0.0123**	**0.0121**	**0.0143**	**0.0140**	**0.0137**

In addition to the nominal conductance calculations, an uncertainty analysis was also done to incorporate the measurement errors into the final conductance values. The calculations done only take into account the bias error due to the accuracy of the measurement devices, and do not include any precision error. The conductances were calculated using the current of each heater circuit and resistance of each heater, as shown more explicitly in Equation 1.

$$G = I^2R / \Delta T \tag{1}$$

In Equation 1, G is the thermal conductance, I is the heater current, R is the heater resistance, and ΔT is the temperature difference across each isolator pair. The heater currents for each circuit were measured directly by each power supply itself, the heater resistances were each measured using a handheld Fluke 115 True RMS Multimeter, and the heater plate and adapter plate temperatures were measured using RTDs. The measurement uncertainties of these devices are tabulated in Table 11.

Table 11: Uncertainties of Measurement Devices

Measurement Device	Measurement Parameter	Uncertainty
Fluke 115 True RMS Multimeter	Resistance	± (0.9% + 1 count)
Keysight E3645A DC Power Supply	Readback Current	± (0.15% + 5 mA)
Class "B" RTD Sensor	Temperature	± 0.12 Ω (± 0.3°C)

The measurement uncertainties of each device were evaluated for each test case. On average, the heater resistance uncertainty was about +/- 0.2 Ω, the current uncertainty was about +/- 0.006 A, and the temperature uncertainty was about +/- 0.2°C. These uncertainties were combined together in an RSS analysis to propagate the errors into the final conductance errors, as shown in Table 12.

Table 12: Final Isolator Conductance Values with Uncertainties

Value	Vacuum -30°C	Vacuum -50°C	Vacuum -70°C	CO_2 -30°C	CO_2 -50°C	CO_2 -70°C	GN_2 -30°C	GN_2 -50°C	GN_2 -70°C
G10 Isolator Conductance									
Nominal Value (W/K)	0.0068	0.0066	0.0064	0.0076	0.0075	0.0073	0.0094	0.0093	0.0092
Uncertainty (W/K)	± 0.0003	± 0.0003	± 0.0003	± 0.0004	± 0.0003	± 0.0003	± 0.0004	± 0.0004	± 0.0003
Ti Isolator Conductance									
Nominal Value (W/K)	0.0116	0.0113	0.0112	0.0125	0.0123	0.0121	0.0143	0.0140	0.0137
Uncertainty (W/K)	± 0.0004	± 0.0004	± 0.0004	± 0.0005	± 0.0004	± 0.0004	± 0.0005	± 0.0005	± 0.0004

The calculated G10 vacuum conductance, when extrapolated to the appropriate temperature, was about 30% higher than the correlated G10 vacuum conductance from the EDU test. This disparity between the two results was not unexpected – since the contact resistance between the fastener and the adjacent hardware was not as low as originally estimated, the conductance of the isolator was much more sensitive to the areas of contact between the fastener and the interfacing hardware, as well as to the applied contact pressure at these regions. This effect was particularly pronounced in the vacuum cases, where there was no additional gas conduction benefit to short out the internal isolator interfaces. One of the problems this lead to was that the installation of the isolators was not as repeatable. Because of the sensitivity of the G10 isolator conductance to the configuration in the vacuum case, it was difficult to get a consistent thermal performance across various test setups. Although the isolators were torqued to approximately the same load, the tolerances of the camera/bracket from the EDU test and the heater/adapter plates from the isolator test were not consistent. Additionally, three isolators were tested in the EDU test while only two were tested in the isolator test, further changing the overall tolerance stack up. With the G10 isolator design, there was also no mechanical way of ensuring that the fastener and G10 isolator were perfectly centered. Doing so would have helped reduce much of the uncertainty of the interfacing contact surfaces. Again, all of these minute details would normally not matter as much if the fastener truly ended up being well-coupled to the adjacent hardware.

Because of the potential uncertainties between the two tests, the dissimilar G10 vacuum conductances were deemed acceptable. There was also the rationale that the truly important results to verify were the GN_2 conductances. During the EDU test, three thermal characterization test cases were done in GN_2: a transient warmup to steady state, a steady state case, and a flight-like warmup/maintenance heating case. The results of the transient and steady state correlations were fed into the warmup and maintenance heating case. Correctly correlating the GN_2 results over the vacuum results was most important because the warmup and maintenance heating that was tested is much closer to what would happen during flight (in CO_2). The purpose of the vacuum testing was to help inform the effects of gas convection and gas conduction. In general, doing so makes the correlation easier but it is not absolutely necessary.

The calculated and extrapolated G10 conductance in GN_2 (0.009 W/K) matched up extremely well with the correlated G10 conductance in GN_2 from the EDU test (0.0089 W/K). The two values only differed by ~1%, which was a nice intuitive validation of why the vacuum conductances did not match up. With the addition of gas conduction inside the isolator, all the uncertainties in the contact areas of the fastener become null as the gas simply thermally shorts out those sections. It is also important to note that the original correlated 0.0089 W/K value was not a random guess – that value was determined based on hand calculations that were done to see what affect gas conduction might have inside the G10 thermal isolator if the fastener were otherwise decoupled from the camera/bracket. Since the fastener was not in perfect contact with the camera as previously assumed and the contact conductance is primarily driven by gas conduction, this approach helped quantify a reasonable approximation of how gas conduction might affect the overall isolator conductance.

The Ti isolator conductance in all test cases was expected to be between ~0.011 W/K and ~0.014 W/K, and the final conductances were indeed within this range. The minimum conductance was 0.0112 W/K in the -70°C vacuum case, and the maximum conductance was 0.0143 W/K in the -30°C GN_2 case. The conductance in CO_2, which was most important, averaged out to about 0.0123 W/K.

IV. Lessons Learned

- For the thermal cycling portion of the EDU test, TC connections were installed directly to a feedthrough plate, instead of with a bulkhead connector as an intermediate interface. This resulted in several instances during checkouts in which either the TC connections at the feedthrough weren't seated properly or the pins were being shorted out against one another. For the warmup characterization portion of that test, a bulkhead connector was used instead and it worked extremely well.
- Taking images and documenting the assembly of the test article and setup was critical. During the model correlation, there was some difficulty in getting the electronics and PRT temperatures to correlate within a reasonable margin. Not shown in the CAD design was a bundle of copper wires soldered from the middle board into the connector on the camera housing, right next to where the TC for the PRT was. Without images of the actual unit, this key thermal path wouldn't have been discovered and the correlation of these components would have been unnecessarily difficult.
- During the EDU GN_2 steady state warmup, the atmosphere TC noticeably rose in temperature as the camera approached steady state. The atmosphere TC was located directly above the camera, so it was warmed by the gas in the camera's vicinity. In the future, it could be beneficial to consider putting multiple thermocouples to characterize atmospheric gradients in a chamber, particularly if there is a large heat load on the test article or if a shroud has large gradients. The temperature rise on the atmosphere TC was only about 3°C, so for this test in particular the lack of several atmospheric thermocouples was not a significant issue.
- For the sake of consistency and to be able to replicate this test setup accurately, all bolted joints should have been torqued to their proper values. This was done for all the camera fasteners, but not for any of the GSE fasteners nor the G10 thermal isolators.
- By far, the most significant lesson learned was to be cautious when developing a thermal isolator design that is meant to replicate the isolation of another design. If possible, it would be best to just use the actual design instead of developing an alternate one. An alternate design adds another level of uncertainty during the model correlation. While the flight-like isolators weren't available at the time to use during the EDU thermal test, there were some improvements that could have been made to the design to make its conductance more deterministic. For example, this isolator design involved G10, whose thermal conductivity is anisotropic and dependent on the manufacturing process. Using another material whose properties are more well-defined would have been beneficial, though not absolutely required. Furthermore, some adjustments to the actual design could have been done to reduce some of the uncertainties in the heat paths through the isolator. For example, as previously mentioned, there were some incorrect assumptions about the conductance through the fastener and through the

G10. To rectify this, the design could have been improved to completely thermally isolate the fastener from the rest of the isolator configuration.

V. Flight Predictions

At the time of the publication of this paper, the Mars 2020 rover landing site was down-selected to Jezero Crater (18.5°N), which has a more benign thermal environment over the worst-case landing site assumed for the thermal design, Holden Crater (26°S). However, for a baselined comparison against the thermal predictions before all the thermal testing[1], this section covers updated predictions for a Holden Crater landing site, not Jezero Crater. WCC and WCH post-correlation predictions are shown in Table 13.

Table 13: Post-Correlation Flight Predictions for Holden Crater

	WCC, 15 m/sec Wind		WCH, No Wind	
Camera/Location	**Warmup Time, minutes**	**Warmup Energy, W-hr**	**Max. Camera Housing Temperature, ˚C**	**Max. Lens Temperature, ˚C**
Front HazCams	28	9.2	38.7	38
Rear HazCams	27	9	37	36
NavCams	21	6.9	24	23
CacheCam	21	6.9	22	23

Under WCC conditions (Holden Crater winter, 15 m/s wind) the longest camera warmup time is 28 minutes and occurs on the front HazCams. The analogous highest warmup energy is 9.2 W-hr. The rear HazCams warm up in 27 minutes and the NavCams and CacheCam each take 21 minutes. When compared against the pre-correlation warmup characteristics and with the same assumptions as before[1], these warmups take about 17% less time and energy. As part of the thermal design process, the goal was to keep the warmup time of the EECAMs under 30 minutes, which has been met with the post-correlation flight predictions.

Under the same WCH conditions as previously assumed[1] (Holden Crater summer, no wind) the max housing temperatures of the EECAMs increase by about 3°C and the lens temperatures increase by 3-4°C. This change is mostly driven by the lower titanium isolator conductance than what was previously assumed for the thermal design. However, the power dissipation of the camera electronics is low enough that these slightly hotter temperatures are not significant drivers.

VI. Conclusion

All the test objectives of the EECAM EDU Thermal Test and EECAM Thermal Isolator Test were successfully met. The camera electronics' functionality was successfully proven at their qualification temperature limits of 70°C and -70°C and sufficient thermal balance data was obtained to correlate a detailed EECAM thermal model. For the most part, the various EECAM components are much more thermally coupled to one another than previously assumed, and the camera as a whole is much more isothermal than expected. This allowed for a lot of reduction in the conservatism of the model. The measured conductance of the G10 isolator that was developed for the EDU test was shown to match strongly with the GN_2 correlated value, differing by ~1%. The measured G10 conductance in vacuum was shown to be ~30% off from the EDU correlated value – however, this deviation has been attributed to and justified by the differences between the two setups involving the isolators. As such, the EECAM EDU correlations were shown to be sound, with no concerns in the final correlated parameters. The measured conductance of the titanium isolator, 0.0123 W/K, was exactly in the expected range that was determined via hand calculations and model runs. The design of these titanium isolators has been shown to be extremely robust – its performance is very independent of atmosphere and temperature, and is easily verifiable with simple hand calculations. With these updated interface conductances and correlations of the EECAM EDU, the EECAM thermal design has shown to be resolute when evaluated under Mars environments. These tests provided enough risk reduction that the EECAM flight units will likely be able to go through protoflight testing and the rover STT without thermal issues.

Acknowledgments

The camera testing discussed in this paper was carried out at the Jet Propulsion Laboratory, California Institute of Technology, under a contract with the National Aeronautics and Space Administration. The authors would like to thank several people from the EECAM subsystem who helped in the planning and execution of these two thermal tests, including, but not limited to, Lauren Montemayor, Reg Willson, Djuna Copley-Woods, Glenn Sellar, Dennis Lee, and Colin McKinney. The authors would also like to thank Jackie Lyra, Eric Sunada, and Ben Furst for their assistance in the test planning and setup. Copyright 2019 California Institute of Technology. U.S. Government sponsorship acknowledged.

References

[1]Novak, K., Kempenaar, J., Redmond, M., Bhandari, P., "Preliminary Surface Thermal Design of the Mars 2020 Rover," *45th International Conference on Environmental Systems*, Bellevue, WA, July 2015.

[2]Kempenaar, J., Novak, K., Redmond, M., Farias, E., Singh, K., Wagner, M., "Detailed Surface Thermal Design of the Mars 2020 Rover," *48th International Conference on Environmental Systems*, Albuquerque, NM, July 2018.

[3]Singh, K., Kempenaar, J., Novak, K. S., "Thermal Development of the Mars 2020 Enhanced Engineering Cameras," *47th International Conference on Environmental Systems*, Charleston, SC, July 2017.

[4]Bhandari, P., Karlmann, P., Anderson, K., Novak, K., "CO_2 Insulation for Thermal Control of the Mars Science Laboratory," *41st International Conference on Environmental Systems*, Portland, OR, July 2011.